actuators

MDPI

Article

Re-Engineering a High Performance Electrical Series Elastic Actuator for Low-Cost Industrial Applications

Kenan Isik [1,*], Shunde He [2], Joseph Ho [2] and Luis Sentis [1]

[1] Department of Mechanical Engineering, The University of Texas at Austin, Austin, TX 78712, USA; lsentis@austin.utexas.edu

[2] PI Electronics, 30 Qin Fu Road, Jin Tang Industrial District, Liu Yue, Heng Gang, Shenzhen 518173, China; he_sd@pie.com.hk (S.H.); ho_kp@pie.com.hk (J.H.)

* Correspondence: kisik@utexas.edu; Tel.: +1-412-641-0905

Academic Editor: Jose Luis Sanchez-Rojas

Received: 8 October 2016; Accepted: 10 January 2017; Published: 22 January 2017

Abstract: Cost is an important consideration when transferring a technology from research to industrial and educational use. In this paper, we introduce the design of an industrial grade series elastic actuator (SEA) performed via re-engineering a research grade version of it. Cost-constrained design requires careful consideration of the key performance parameters for an optimal performance-to-cost component selection. To optimize the performance of the new design, we started by matching the capabilities of a high-performance SEA while cutting down its production cost significantly. Our posit was that performing a re-engineering design process on an existing high-end device will significantly reduce the cost without compromising the performance drastically. As a case study of design for manufacturability, we selected the University of Texas Series Elastic Actuator (UT-SEA), a high-performance SEA, for its high power density, compact design, high efficiency and high speed properties. We partnered with an industrial corporation in China to research the best pricing options and to exploit the retail and production facilities provided by the Shenzhen region. We succeeded in producing a low-cost industrial grade actuator at one-third of the cost of the original device by re-engineering the UT-SEA with commercial off-the-shelf components and reducing the number of custom-made parts. Subsequently, we conducted performance tests to demonstrate that the re-engineered product achieves the same high-performance specifications found in the original device. With this paper, we aim to raise awareness in the robotics community on the possibility of low-cost realization of low-volume, high performance, industrial grade research and education hardware.

Keywords: series elastic actuator; re-engineering for low-cost; industrial automation

1. Introduction

Safety is becoming a key design requirement for collaborative robots and automation systems with expected growth in industrial manufacturing and emerging service applications. SEAs are often being considered to improve those safety requirements because of their mechanical and force sensing properties. In particular, new industrial applications are trying to bring robots and people together in the same workspaces for improved productivity through enhanced collaboration (Co-Bots) and physical human-robot interaction (pHRI). Beyond manufacturing, Co-Bots are expected to play a disruptive role in our day-to-day lives boosting our levels of productivity, comfort, health, and security.

In typical industrial manipulators, there is the traditional premise that the stiffer the mechanical interface between the actuator and the load, the better it is [1]. Although this premise has made industrial robots hugely successful due to their position controllability, it leads to humans and robots being physically separated as a safety precaution. Stiff actuators are best suited for position

control applications where the robot environment is almost perfectly known. On the other hand, the environments where humans work are dynamic and unstructured, requiring the use of force sensing and control techniques for safe pHRI. Force sensing and control can be achieved by using load cells but the rigid interface between the motor and the load will remain a safety concern due to the reflected inertia of rotors in electrical actuators.

SEAs have several key benefits such as reducing the effect of the reflected inertia, higher tolerance to impact loads, passive mechanical energy storage, low mechanical output impedance, and increased peak power output [1–3].

In addition to increasing the safety factor during a pHRI, SEAs are a good solution for handling fragile materials under uncertainty. Current robot manipulators use high precision position control for these types of applications, which require a well-determined workspace. A small position error at the end-effector can easily damage the materials because of the high forces exerted by the stiff joints. Using SEAs allows us to quickly provide compliance upon impact to protect the objects being manipulated. As such, SEAs could become an important technology to cut costs due to material mishandling.

Because of these benefits, there has been a large research focus on design and control of SEAs. SEA hardware typically consists of three main components: an electric or hydraulic motor to deliver mechanical power, a drive-train to amplify the motor torque, and an elastic element for both sensing the output force and providing passive compliance to the output. Many combinations of these components have been considered over time.

Compact and lightweight designs are important for legged robots and human assistive systems. In [4–6], the authors use harmonic drives for speed reduction and custom-made planar springs as elastic elements. Harmonic drives are good for reducing backlash and keeping the actuator compact and lightweight. However, they suffer from poor backdrivability and high cost. Since the number of engaged gear teeth is low, harmonic drives are prone to ratcheting and buckling under high loads. Custom designed planar springs are beneficial for compact, rotational SEA designs but are harder to manufacture and therefore lead to cost increases. In [7,8], compactness is achieved by using bowden-cable based design and separating the actuators from the output joints. The main drawback of bowden-cable systems is their hard-to-model nonlinearities which make them difficult for precision control. One of the first designs of SEAs [9], presents a simple and compact design based on linear die springs with a rotational gear. The effect of the collocation of the spring was analyzed in [10]. This focus on compactness has been a motivation for our design.

In [11,12], the spring is located within the speed reduction mechanism. Such designs allow for lighter springs since the torque on the spring is lower than at the output. In [13], elasticity is created via parallel linear springs of different stiffness. This design significantly reduces the required motor torque and increases the efficiency. In [11,14], the authors use a worm-gear mechanism for speed reduction which allows the motor to be orthogonal to the joint axis. These designs are more suitable for knee orthosis.

A novel, rotary spring design for a compact SEA was presented in [15]. The rotary elastic component of this SEA is created by using a novel arrangement of linear springs. While this design is a low-cost alternative to high-priced custom planar springs, it suffers from nonlinear stiffness.

By using variable stiffness and nonlinear springs, the range of applications and control capabilities of SEAs can be extended. There has been major research on the benefits of adjustable [16–21] and nonlinear [22] stiffness springs. Also, a novel spring mechanism with an infinite range of stiffness was proposed in [23] for SEAs. Like the effect of variable stiffness, the effect of variable physical damping [24] and continuously-variable transmission [25] has been studied.

In [26–30], the authors use a ball-screw mechanism for speed reduction for prismatic SEA designs. Ball-screw mechanisms are highly efficient (90%), highly backdrivable, have a high tolerance for impact loads, and do not introduce torque ripples. Therefore, ball-screw mechanisms are good candidates for high-efficiency actuator designs. An important drawback of using a ball-screw mechanism is the fact that an output mechanism is needed for converting the prismatic output to rotation when necessary.

In [31–33], the authors use off-the-shelf components for designing SEAs which is an important strategy to keep the costs low. The authors use a planetary gearbox for speed reduction in their designs. Planetary gearboxes have low efficiency and poor impact tolerance due to their low backdrivability. Torque ripple and backlash are other drawbacks of planetary gearboxes.

A low-cost robotic arm with SEAs was presented in [34]. In order to reduce the total cost, stepper motors, which are relatively cheaper and provide high torque at low speeds, were used. High motor torque eliminates the necessity of a high gear ratio speed reduction mechanism and, thus, reduces the cost and weight of the robot arm, while low motor speed limits the maximum joint velocity. The pHRI safety was achieved by using SEAs but only the proximal four joints have SEAs in order to keep the total cost low. The series elasticity and force sensing of the SEAs were achieved by using polyurethane tubes which is another important step to reduce the cost. The main drawback of polyurethane tubes is their nonlinear stiffness behavior with significant hysteresis. In [35], the authors propose a low-cost SEA for multi-robot manipulation applications. The authors use planetary gearbox along with a capstan drive. The angular position at the joint is measured with a potentiometer. The compliance is achieved with a thin strip of spring steel. The overall cost is kept low by designing the custom parts with simple geometries. In [36], a modular and low-cost variable stiffness actuator was proposed which is designed to serve as a building block for low-cost multi degrees of freedom robot designs.

Although many different design configurations of SEAs have been investigated, low-cost realization of SEAs with a focus on high-performance and industrial grade strength have not been studied. Reducing the cost of SEAs without compromising too much on the performance is necessary for the industrial and educational SEA designs. The total service life with minimal maintenance or part replacement is another important design consideration. Although there are low-cost industrial robot arms with SEAs such as Baxter [37] which benefits from reduced unit cost due to high-volume production, low-volume research hardware preparation with low manufacturing cost needs to be explored.

Designing SEAs with low cost and long service life is also important for their use in education. The actuators designed for research have a limited time of use and are built with high-end components without the cost in mind. On the other hand, the systems designed for education purposes require longer service life with limited maintenance and affordability for increased accessibility.

In this paper, we devise a low-cost SEA which has comparable force and position tracking performance to the high-end SEAs while providing industrial level service life. As a reference point, we chose 40,000 h of expected service life and half of the cost of the SEA that we chose to re-engineer. In order to achieve these performance points, we reduced the number of custom parts and selected off-the-shelf parts with the targeted service life. We designed the custom parts with simple geometries which can be prepared with minimal machining. We partnered with an industrial company in China for finding both the right components for industrial applications and the lowest possible prices for the off-the-shelf components. Manufacturing in China is much cheaper not only for mass production but also for individual projects. Some of the various reasons why manufacturing in China is cheaper is the fact that the average labor cost is still lower than in the United States, high raw material production, low raw material pricing and government policies on low shipment cost [38]. Using these aforementioned methods, we show that the cost of low-volume mechatronic hardware preparation for research in academia, education and industrial settings can be lowered drastically while keeping the quality reasonably high and compromising on some of the less important design aspects, weight in our case.

Lowered costs will increase the availability of robots to the broader population and more research availability will boost the development of robotics applications. The rest of this paper is organized as follows: In Section 2, the design process of the StoneAge-SEA (SA-SEA) is explained. Modeling, force and position controllers are given in Section 3 and the performance on force and position control as well as impact detection tests are presented in Section 4. Finally, additional information about the proposed procedures and results are discussed in Section 5.

2. Design

Setting the design goals for the desired application is a crucial step for keeping the costs low. Only the necessary properties of the system should be taken into consideration and their priorities should be properly sorted. For example, the energy density is an important design aspect for the SEAs designed to be used for humanoid robots or orthosis systems while it has a lower priority for industrial setups since they are usually rigidly grounded. For our design, maximum output speed, continuous output force, cost, backlash, bandwidth, mechanical strength, service life and human safety are the important considerations. For the sake of mechanical strength and long service life, the weight of the actuator is considered as low priority.

Target output speed and force values are taken from the re-engineered model, UT-SEA. While keeping the force and position control performance comparable to the UT-SEA, we targeted half of the cost for the new SEA. Table 1 shows the available properties of the UT-SEA and targeted and achieved values of the new SA-SEA.

Table 1. Properties of the UT-SEA [26], our design goals and achieved properties of the SA-SEA.

Design Aspect	UT-SEA	Target Value	SA-SEA
Cont. Output Force	848 N	848 N	829.96 N
Peak Output Force	2800 N	2800 N	2355.47 N
Peak Output Speed	32.5 cm/s	32.5 cm/s	28.8 cm/s
Cost	$5100	< $2550	$1750
Force Bandwidth	18 Hz	10 Hz	8.5 Hz
Expected Service Life	N/A	40,000 h	>60,000 h
Force Sensitivity	0.31 N	0.31 N	0.06 N
Stroke	6 cm	6 cm	7.1 cm
Weight	1168 g	N/A	3280 g

After setting the force and speed goals, the selection of the speed reduction mechanism is a critical step for the overall performance of the system. The system's mechanical efficiency and backlash are mainly affected by the speed reduction mechanism. Backlash is an undesired property for most of the engineering systems and the existence of backlash adversely affects system stability and repeatability. Harmonic drives and ball-screw mechanisms are the best solutions for backlash problems. Between the two, ball-screw mechanisms are more durable against excessive forces and impact loads. The typical efficiency of the ball-screw mechanisms is in the order of 90% whereas the typical efficiency of harmonic drives is in the order of 80%. Ball-screw mechanisms are also cost effective solutions for linear motions and are therefore a good candidate for a low-cost SEA.

There are two stages of speed reduction in the SA-SEA which are the ball-screw mechanism and the pulley system. Since the ball-screw mechanism is a more expensive component than the pulley system and has a greater possibility of cost reduction, we selected the ball-screw mechanism first and then selected the pulley ratio accordingly in order to meet the design requirements. We kept in mind that having a high pulley ratio will affect the overall actuator size. By using Equation (1) and using a maximum pulley ratio of 3:1, we selected the BSHR01205-3.5 model ball-screw mechanism from TBI Motion (New Taipei City, Taiwan) which requires less than 0.5 Nm input torque for the desired force output. We set this maximum torque value in order to keep the cost and size of the motor under reasonable values. In the following equation, (T) is motor torque, (F) is force output, (l) is ball-screw lead, (N) is pulley ratio, and (η) is ball-screw mechanism's efficiency.

$$T = \frac{F\,l}{N\,2\pi\,\eta} \tag{1}$$

The selected ball-screw mechanism requires 0.25 Nm of motor torque if we choose the 3:1 pulley ratio in order to match the continuous force output target. For cost reasons, we decided to use an AC servo motor and selected the TS4603 model from Tamagawa Seiki Co., LTD (Iida, Japan) with

0.318 Nm continuous torque output. The selected motor driver is compatible with Programmable Logic Controllers (PLCs) and has its own Proportional–Integral–Derivative (PID) controller both of which are widely used in industrial control applications. The price for the torque was the main consideration for motor selection.

Solving the Equation (1) for N with the given rated torque and specifications of the selected ball-screw mechanism gives a pulley ratio of 2.36. Considering the available pulley teeth numbers, the desired mechanical strength of the pulleys and the suitable timing belts, we selected a 60:26 timing pulley ratio, which gives slightly lower output values than the desired ones.

The peak output force with the selected motor and assumed drive-train efficiency (95% for the pulley system and 90% for the ball-screw mechanism) was calculated to be 2355 N for the chosen system parameters. The spring should reach this force value before reaching its shut length. Using soft springs allows higher force sensing resolution since the distance traveled for the same force will be longer. On the other hand, softer springs reduce the bandwidth of the system. Having these in mind, we selected the TL50-060 from Tohatsu Springs (Tokyo, Japan) which has 137.96 N/mm stiffness. Since two springs are used in series, the effective spring stiffness is expected to be 275.8 N/mm. With 10 mm allowed working distance after pre-compression, this stiffness is high enough to hold the maximum peak force created by the motor.

For force sensing, the linear motion of the spring is converted to rotational motion by using a pulley system. After setting the allowed working distance of the spring, there are two variables affecting the force resolution. These are the sensor resolution and the diameter of the pulley used at the sensor shaft. By considering the minimum number of teeth available for the timing pulley, we selected the 17-bit TS5667N120 from Tamagawa Seiki Co., LTD. (Iida, Japan) which provides 0.06 N force resolution. This is a low-cost absolute encoder with RS-485 NRZ communication protocol which has great immunity to the noise in industrial environments and has fast data transfer rates as high as 50 MBaud.

The force sensing mechanism was also re-engineered to be more durable and easily calibrated. The number of encoders was reduced to one from two which contributes to cost reduction. The selected encoder significantly increases the force sensing resolution. Figure 1 shows the force sensing mechanism of the SA-SEA.

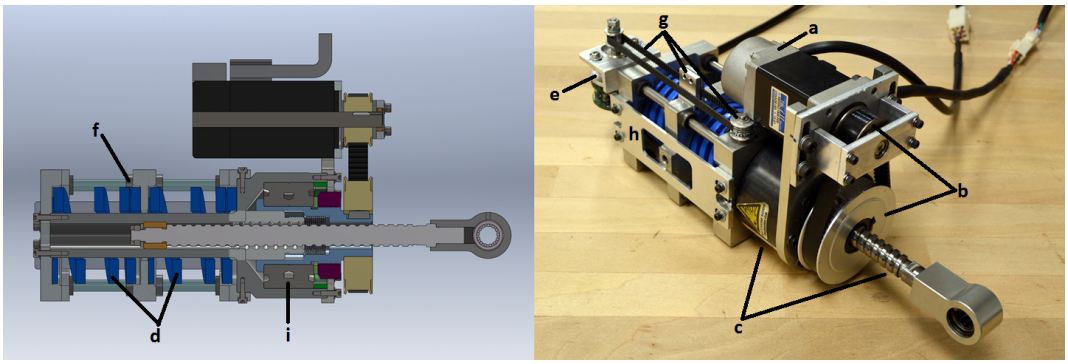

Figure 1. The SA-SEA and its cross section showing (**a**) Tamagawa Seiki Co., LTD TS4603 motor; (**b**) 60:26 pulley system; (**c**) TBI Motion BSHR01205-3.5 ball-screw mechanism; (**d**) Tohatsu Springs TL50-060; (**e**) Tamagawa Seiki Co., LTD TS5667N120 17-bit absolute encoder; (**f**) Misumi BGSTZ6-90 miniature ball bearing guides; (**g**) Force sensing mechanism; (**h**) Side bracket for easy assembly and rotational stiffness; (**i**) Misumi B7006-DB angular ball bearings.

The expected service life of the actuator heavily depends on the ball-screw mechanism which is the component that is the most prone to deterioration over time. There are many aspects affecting the service life of the ball-screw mechanism. For instance, proper lubrication, assembly, and operation as well as environmental variables such as dust are factors affecting service life.

We calculated the service life of the ball-screw mechanism by assuming that the actuator output is making a sinusoidal motion with the highest continuous actuator output speed. We also assumed that a sinusoidal axial load with an amplitude matching the maximum continuous force output of the actuator will be applied. By using Equation (2), the expected service life is calculated to be 60,894 h. Since SEAs increase the lifetime of drive-train components, the expected service life of the ball-screw mechanism is higher than the calculated value. In Equation (2), L_t is the expected life of the ball-screw mechanism, C_a is the basic dynamic load rating which is taken from the component datasheet, P_e is the average axial load (65% of the maximum load for sinusoidal motion), f_w is the load factor (1 for very low vibration and impact conditions), and n is the average rotational speed (65% of the maximum speed for sinusoidal motion).

$$L_t = \left(\frac{C_a}{P_e\, f_w}\right)^3 10^6\, \frac{1}{60\, n} \tag{2}$$

All other off-the-shelf components such as bearings and timing belts are selected by considering the targeted service life of the actuator and its cost-effectiveness. The custom parts are designed to minimize the machining time of the aluminum plates and ease the assembly of parts. In order to make the assembly process easier and to add torsional stiffness to the actuator body, side plates are added to the design (h in Figure 1).

On the controller side of the actuator, we used a PC-104 based embedded PC with RTAI Linux. The real-time control loop is set to run at 1 kHz while the sensor data is updated at 2 kHz on a separate thread. The PC-104 stack includes a DAC board for commanding desired motor torque and a serial communication board for interfacing the encoders.

3. Modeling and Control

There are two types of control mode discussed in this paper. These are force control and joint position control. Our goal in force control mode is to achieve a near ideal force source behavior from the SA-SEA and accurately track dynamically changing desired forces in the targeted bandwidth. For the joint position control, the goal is to follow the rapidly changing desired joint positions accurately. The position controller was built on top of the force controller by using it as a building block. In order to achieve high performance from the controller, it is important to build a good model of the system and characterize the system components. In this section, we present the modeling of the SA-SEA, characterization of the spring, and development of the control architectures.

3.1. Modeling

There are two fundamental SEA structures. These are referred to as Force Sensing Series Elastic Actuator (FSEA) and Reaction Force Sensing Series Elastic Actuator (RFSEA) [26]. Figure 2 shows the simplified models of FSEA and RFSEA. The re-engineered SEA in this study has the RFSEA structure. Compared to prismatic FSEAs, RFSEAs are more compact and have a larger range of motion. In RFSEA designs, the spring is located between the motor and the ground. Therefore, the load is directly connected to the gear train. While this reduces the impact tolerance, compensation is provided by the high impact tolerance of the ball-screw mechanism. Another drawback of RFSEA is the larger sprung mass which includes the mass of the motor, inertia of the rotor and the gear train. This results in a more complex force calculation for the RFSEAs. For FSEAs, the output force can be calculated directly from spring deflection whereas for RFSEAs, the force seen at the output is the sum of the inertial force of the sprung mass of the actuator, the force due to the effective friction in the system, and the spring force. Figure 3 shows the general model of the SA-SEA which shows the system components affecting output force.

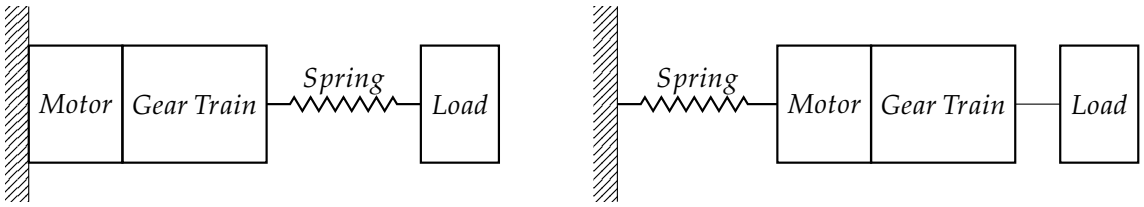

(a) FSEA **(b)** RFSEA

Figure 2. Simplified models of FSEA (**a**) and RFSEA (**b**).

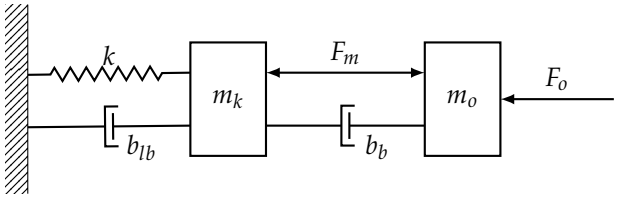

Figure 3. Model of the SA-SEA. Here, k is the effective spring stiffness, b_{lb} is viscous friction at the linear ball bearings supporting the spring cage, m_k is the total sprung mass of the actuator, F_m is the motor force, b_b is the viscous back-drive friction of the ball-screw mechanism, m_o is the output mass and F_o is the output force.

Characterization of the components is important for creating an accurate model of the system. It is especially important for low-cost components since there is a greater chance of having different performance values than the ones given in the datasheets. The characterization process begins with the calibration of the force sensor in order to find the zero force position of the encoder. To to this, we disconnected the actuator from the joint and mounted it horizontally to the table. After calibrating the force sensor, we started our spring characterization process. We kept the output shaft of the joint parallel to the ground, locked the gear train, applied known forces in both directions from 0.3 m distance and recorded the sensor readings. The effect of the output bar's weight has been taken into account. The Figure 4 shows the normalized applied force v.s. sensor readings. As the figure shows, the spring is perfectly linear in the testing range but there is a slight shift on the force readings on y-axis. This shift is introduced by the force bias due to the motor mass sliding on the ball bearings because of its sloped position.

The motor used in this project is an industrial AC servo motor which is designed to be used at relatively high speeds. When the motor is used at high speeds, the rotor inertia acts like a low-pass filter and cancels out the torque ripples seen at the motor output. In force control applications such as gravity compensation, the motor rotates at lower speeds. This makes the torque ripples seen at the output of the low-cost AC servo motors more observable. Figure 5 shows the torque ripples seen at the actuator for a ramp input. These ripples were canceled out by using the PID based force control explained in Section 3.2.

At this point, it is important to point out that we made sure that the ripples seen at spring force originated from the motor. We checked this by observing the torque ripples when the motor was disconnected from the drive train.

Some of the system parameters such as the sprung mass of the actuator and the effective viscous friction in the system are hard to calculate. System identification is a useful tool in order to have an accurate system model. Unfortunately, the high torque ripples prevent a successful open-loop system identification. Therefore, we performed closed-loop system identification by using the proposed force controller in Section 3.2.

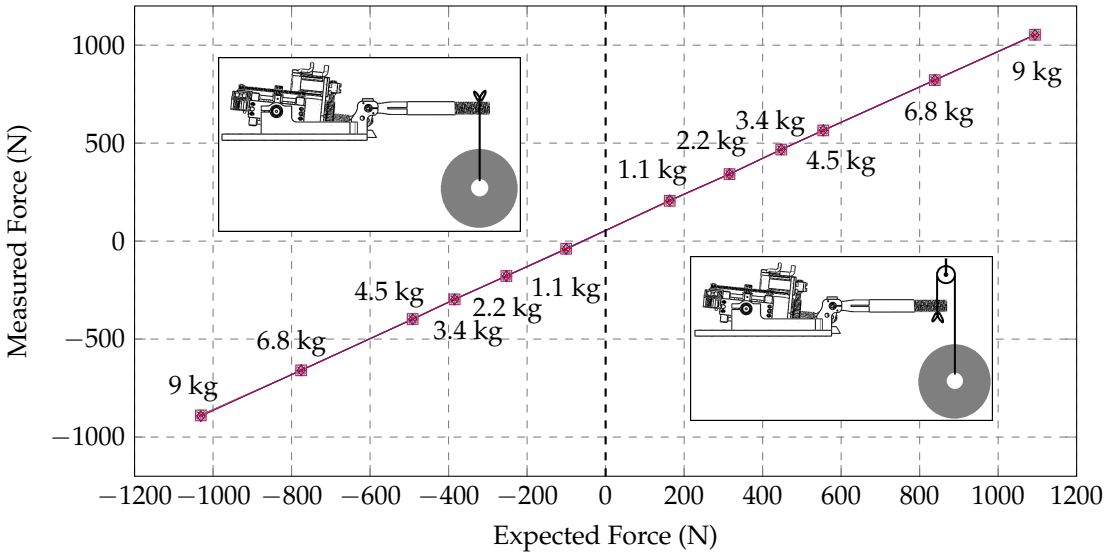

Figure 4. Spring characterization graph. Each experiment was performed 6 times. The graph shows the consistency of the experiment results. The approximate values of the dumbbell weights used in these experiments are: 1.1, 2.2, 3.4, 4.5, 6.8 and 9 kg.

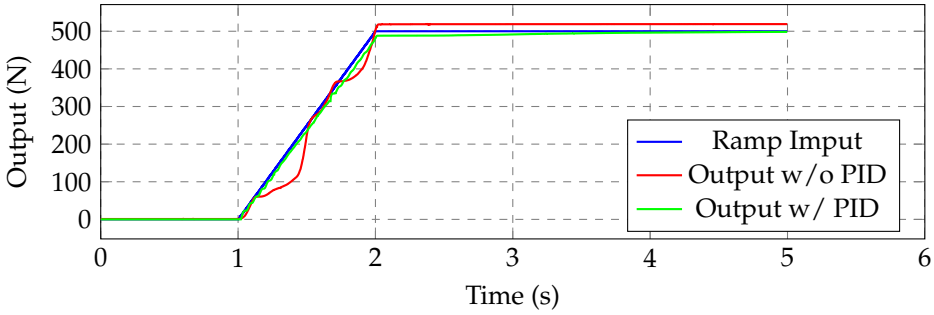

Figure 5. Torque ripple cancellation with PID based force controller.

3.2. Force Control

In order to simplify the force control architecture, we used a high impedance output setup. Figure 6 shows the model of the high impedance setup created by grounding the actuator output. In this configuration, $F_o = F_m + F_{b_b} = F_{m_k} + F_{b_{eff}} + F_k$. As a result, the output force equation can be written as

$$F_o = m_a\ddot{x} + b_{eff}\dot{x} + kx \tag{3}$$

where b_{eff} is the effective viscous friction in the actuator.

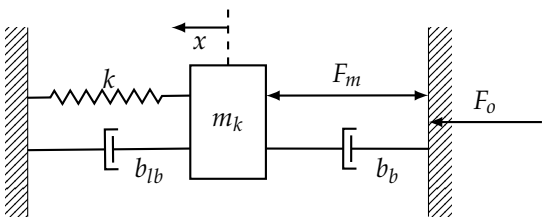

Figure 6. Model of RFSEA for force control with high impedance load.

Equation (3) requires derivation of both $\ddot{x}$ and $\dot{x}$ for an accurate force feedback, especially at high frequencies. Considering the mechanical failure possibility of RFSEA design near resonant frequency [26], we control spring force by using Hooke's Law:

$$F_k = kx \tag{4}$$

This approach sacrifices the accuracy of force feedback at high frequencies but guarantees stable control for a wide range of frequencies. The transfer function between the motor force and the spring force can be written as

$$\frac{F_k(s)}{F_m(s)} = \frac{k}{s^2 m_k + s b_{eff} + k} \tag{5}$$

Equation (5) yields a second order mass-spring-damper system. In this equation, m_k represents the sprung mass of the actuator which includes the inertial elements of the actuator such as the motor mass, the partial mass of the ball-screw mechanism and the springs, as well as the rotational inertia of the rotor. Finding m_k and b_{eff} requires extensive study of the system. In order to find the unknown system parameters, we performed closed-loop system identification by using the force controller shown in Figure 7. We used an exponential chirp signal as F_d and fitted the experimentally found model to Equation (5). By using the known gains and system parameters, we found that $m_k \approx 64$ kg and $b_{eff} \approx 921.6$ Ns/m.

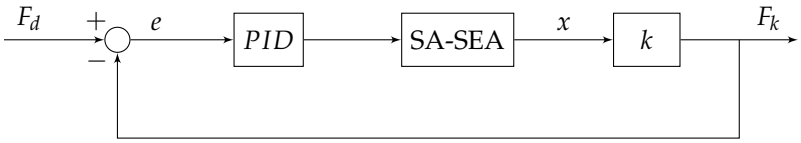

Figure 7. Force controller for high impedance RFSEA setup.

Since we designed the SA-SEA for industrial and educational applications, we only used a PID controller. PID control is a simple and effective control approach used for more than 90% of the industrial control applications. It is also one of the most fundamental control method taught in control education. PID control can be realized by using a PLC which is a common controller selection in industry. Figure 7 shows the force controller used in this study. As it can be seen on the controller diagram, there is no filter applied to the feedback signal. Low noise level on the feedback was achieved by taking advantage of the high noise immunity of the RS-485 communication and the high data update rate of the encoder. This enables multiple sensor readings to be done in one control cycle, eliminating any inconsistent feedback data. The only filter used in this controller is the first order low-pass derivative filter given in [39]. In this control approach, the required motor torque command is calculated from the desired spring force by using the system parameters and is sent to the motor driver.

3.3. Position Control

The second controller designed for the SA-SEA is a joint position controller. In joint position control, the goal is to accurately follow the rapidly changing desired joint positions. After achieving an accurate force control performance, we used the designed force controller as a building block for the position controller. The force created at the actuator output is converted to joint torque using the mechanism shown in Figure 8. The joint torque (τ_a) which is created with the force output of the actuator (F) can be calculated as follows [26]:

$$\tau_a = FL(\theta_a) = F \frac{cb \sin \theta_a}{\sqrt{b^2 + c^2 - 2bc \cos \theta_a}}. \tag{6}$$

Also, the relationship between the joint torque and the load dynamics can be calculated as,

$$\tau_a = J_a\ddot{\varphi} + B\dot{\varphi} + \tau_g(\varphi). \tag{7}$$

In this equation, J_a represents the load inertia, B represents the joint friction and $\tau_g(\varphi)$ represents the torque created by gravity and can be calculated as,

$$\tau_g(\varphi) = m_a g l_{m_a} \cos\varphi \tag{8}$$

where m_a is load mass and l_{m_a} is the distance of the center of the load mass to the joint. The joint angle φ is determined by the joint position sensor and θ_a used in Equation (6) is dependent on joint angle.

Using Equations (6)–(8), the nonlinear equation governing the load dynamics can be written as,

$$F = \frac{\sqrt{b^2 + c^2 - 2bc\cos\theta_a}}{cb\sin\theta_a}[J_a\ddot{\varphi} + B\dot{\varphi} + m_a g l_{m_a}\cos\varphi]. \tag{9}$$

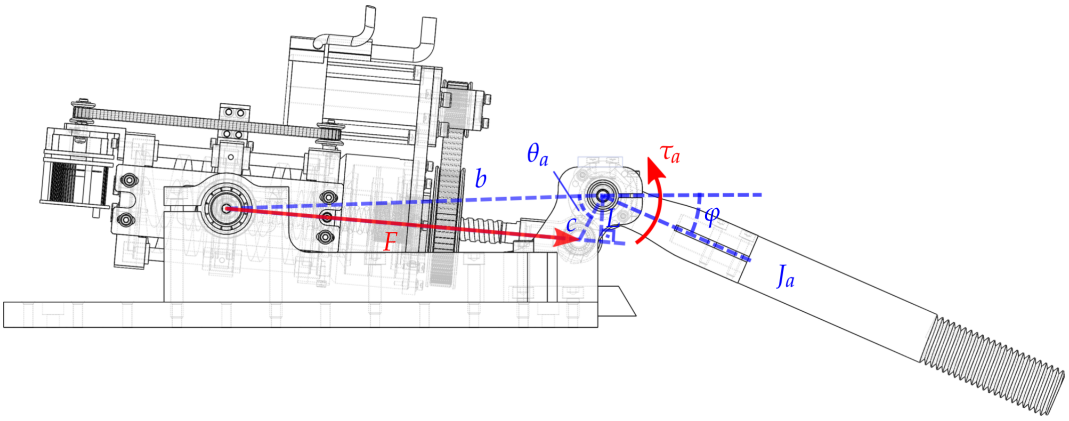

Figure 8. Kinematic structure of the joint link mechanism.

As Figure 9 shows, the required joint torque is derived using the desired joint trajectory plus the gravity effect based on the joint position. The inertial and friction force terms are included as a feed-forward term. The desired actuator force output is calculated by using the inverse of $L(\theta_a)$ and is sent to the force controller.

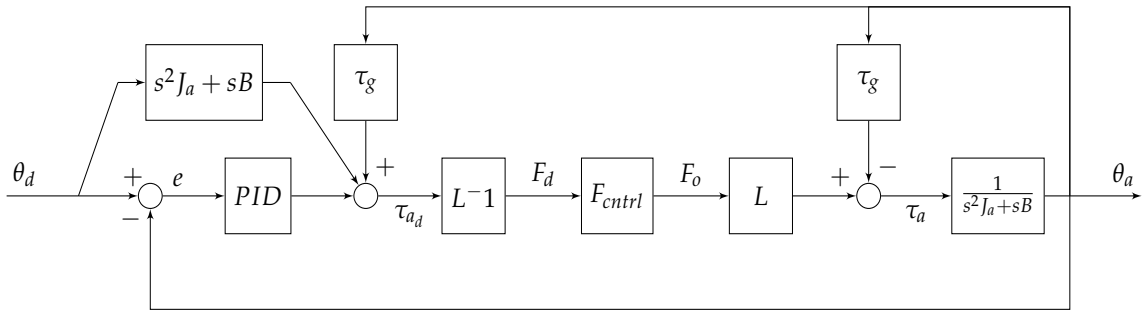

Figure 9. Joint position controller.

4. Performance Tests

The main goal of this study is to achieve high performance from a low-cost SEA. Fundamentally, we aim for comparable performance to the UT-SEA in terms of its force and position tracking capability. These are building blocks for any higher level controllers and directly affect the system's overall performance.

We also performed an impact recognition test in order to analyze the system's mechanical robustness and responsiveness. The performance of the SA-SEA on these tests is critical for its use in industrial applications. The results of the experiments are presented in this section.

4.1. Force Control Test

For force input tracking, the actuator output was rigidly grounded as modeled in Figure 6 and a PID based force controller, which is shown in Figure 7, was used. In order to see the system's response for rapid changes in desired force, we applied an exponential chirp signal with an amplitude of 100 N and a frequency range of 0.1–100 Hz for a 30 s duration. This experiment is necessary in order to see the system's frequency response at high frequencies and to see the force bandwidth of the system.

Figure 10 shows the bode plot of this experiment. As it can be seen, the SA-SEA shows good force tracking performance at lower frequencies and the actuator output degrades at higher frequencies. The bode plot shows that the force tracking bandwidth is 8.5 Hz, which is lower than the targeted bandwidth of 10 Hz. The bode plot also shows that the magnitude values increase at high frequencies instead of decrease, which is due to the high frequency noise on the recorded output data.

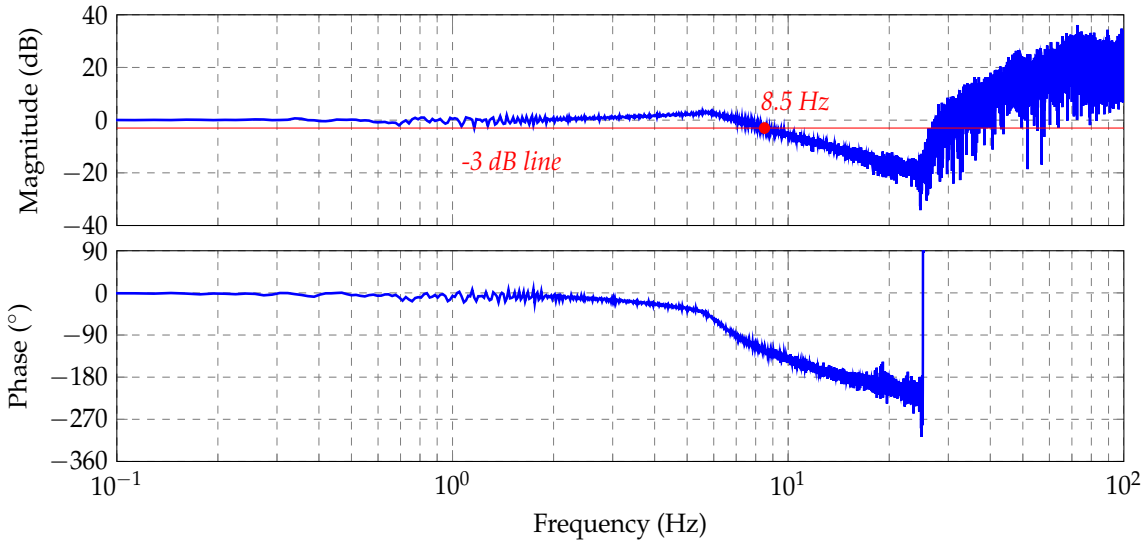

Figure 10. Bode plot of the force tracking test with chirp input (f = 0.1–100 Hz).

The bandwidth of force tracking can be improved by using model-based controllers. For simplicity, we used a PID-based controller only. A higher bandwidth can be achieved by testing the force controller with a smaller amplitude reference signal.

4.2. Position Control Test

Another important performance metric for the SEAs is the joint position control performance. It is necessary to precisely follow dynamically changing desired positions with a small overshoot, short settling time, and low steady-state error values. In order to test the system performance on joint position control, we used the position controller explained in Section 3.3 with a smooth step input featuring a 0.5 rad step height. We attached a 2.268 kg weight at a 20 cm distance from the joint. Figure 11 shows the result of the position control experiment. The system output shows 10% overshoot and 0.35 s settling time for 2% band.

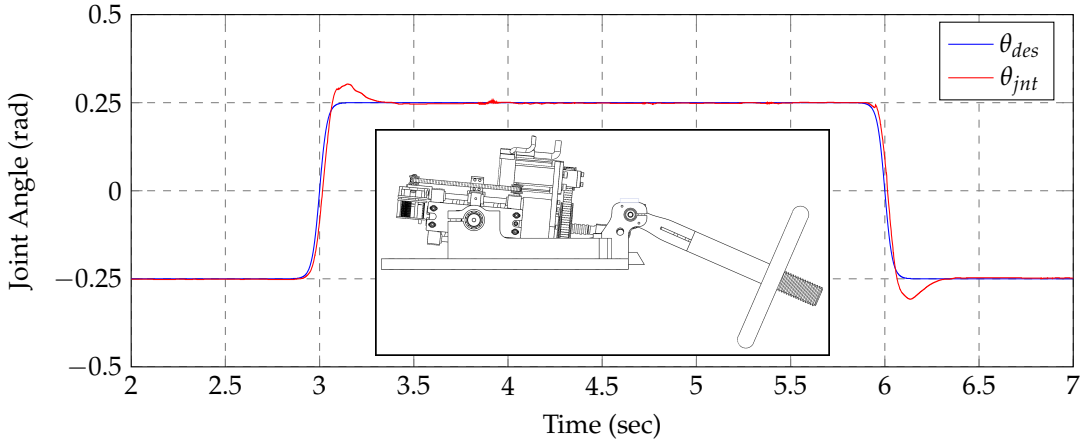

Figure 11. High speed joint position tracking with 2.26 kg load located at 0.2 m from the joint.

4.3. Impact Detection Test

SEAs are inherently safer actuators than the rigid actuators due to the elastic element added between the actuator and the output. The elastic element attenuates the reflected inertia of the rotor and improves safety for the actuator environment while marginally reducing the safety with the possibility of increasing the upper bound of the joint velocity due to the built up kinetic energy on the spring. On the other hand, high-frequency load changes and impact forces are filtered by the elastic element which improves the safety of the actuator itself against mechanical failures in the drive-train.

The safety level of SEAs can be further improved by using sensing and control approaches. SEAs are very good on providing reliable force feedback. This allows us to quickly recognize unexpected force changes at the output and create reactive control approaches in order to improve safety. Haddadin et al. studied different impact detection and reaction methods in [40]. The impact detection methods proposed in [40] are model-based methods and, thus, require extra measures to cope with possible modeling errors. There are many design aspects affecting the safety of a robot such as joint mass, joint speed, joint stiffness, to name a few. In [41], the authors further improve the safety of the robot by avoiding the collision in the first place, then use collision detection and reaction methods if the collision is unavoidable. While taking a proper reaction to the impacts is important, the robot or the actuator should be able to distinguish the user collaboration from an impact. In [41], the collaboration phase starts if a collaboration request comes from the user or the robot.

In this study, we use a simple method for distinguishing the collision from collaboration. We always monitor the joint angle error and the spring force error and use a force error threshold for detecting the impact. When the user pushes or holds the output link, the joint angle error increases but since the desired force is regulated according to the joint angle error, the spring force error does not increase. However, when there is an impact, an instantaneous jump on the spring force error level occurs. This method allows us to safely collaborate with the actuator while monitoring impacts. Figure 12 shows the joint angle of the SA-SEA actuator under normal operation, during collaboration, and under impact. The actuator starts with the normal operation and after the first cycle, the user holds the output link and pushes it around. In this phase, the actuator tries to follow the desired joint trajectory. After letting go of the output link, the user holds his hand in the desired joint trajectory. When the impact occurs, the actuator recognizes the impact and responds to it by moving back to the furthest opposite direction possible. We believe that the safest reaction method is to take all the energy out of the output link as quickly as possible. The proper way to do this is by applying the highest possible torque to the joint in the opposite direction of the motion when the impact occurs. By doing so, all the kinetic energy of the joint link is removed. After this point, switching to gravity compensation mode cancels out the potential energy of the output link and allows it to fully comply to the user's motion. For the sake of demonstrating the quick response of the actuator, we chose to

move the output link in the opposite direction in this experiment. The analysis of the experiment result showed us that the detection of the impact took 11 ms and the total time from the occurrence of the impact to completely stopping the joint link's motion in the impact direction is 55 ms. The joint rotated 4.29° during this time period.

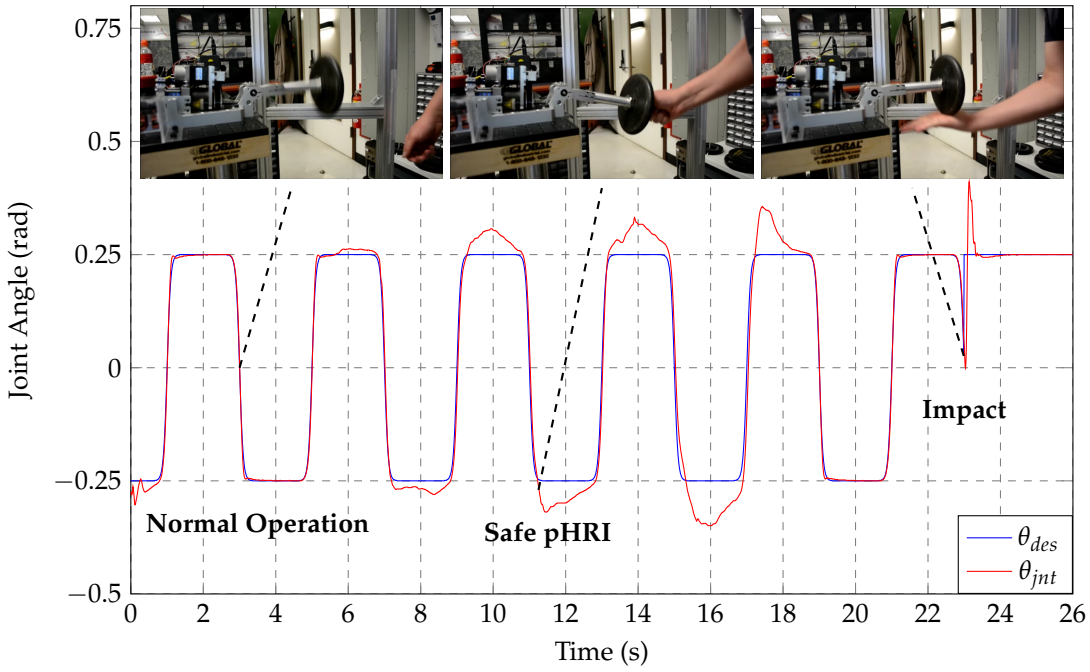

Figure 12. Physical human-robot interaction (pHRI) and impact recognition. The experiment starts with position control. The user interacts with the actuator safely and then causes impact at around $t = 23$ s. The actuator quickly moves to safe position in the reverse direction.

The main drawback of our impact detection method is its dependency on the performance of the force and position control loops. A low-performance controller can easily trigger a safety flag in the system. This can be avoided by setting the threshold values according to the maximum expected force and position errors when there is no impact or user input as long as these values do not pose any danger to the user when impact occurs. It is important to note that this safety check should start after the initial errors at the system startup are phased out.

5. Conclusions

In this paper, we showed that a significant cost reduction on low-volume mechatronic hardware is possible. We significantly reduced the cost of our SEA to one-third of its original cost while maintaining good force and position control performance. This was done by increasing the number of off-the-shelf components, partnering with an industrial company in China for optimal production costs, and carefully designing custom parts for minimal machining work. While reducing the cost, the total mass of the actuator increased. There are two main reasons behind the increase of the total mass. These are the bulkiness of some of the low-cost components and thicker design of the custom parts for sturdy mechanical construction and longer service life.

It is a challenge to make a significant reduction on the cost of an actuator. At the mechanical design phase, increasing the number of off-the-shelf parts helps to reduce the cost, as expected. In order to further reduce the costs, low-cost components should be selected as long as they satisfy the performance requirements. Otherwise, we need to find techniques to compensate for the shortcomings of the components via mechanical design or control methods. The biggest challenge we had working

with low-cost components was the lack of sufficient documentation and technical support. It requires extra effort to get the most performance out of the low-cost components.

The main drawback of the SA-SEA is its low power density. This can be improved by detailed finite elements method analysis on custom parts and reducing their weights. The control performance can be further improved by using model based control schemes. Our future work will be to improve the power density and to design a low-cost SEA which is suitable for mobile platforms. We are also working on devising a methodology for finding the optimal gains for best impedance control performance.

Acknowledgments: This research was funded by PI Electronics Ltd. of Hong Kong and supported by The Ministry of National Education, Republic of Turkey.

Author Contributions: The design of the actuator was performed as a collaborative work between Kenan Isik and Shunde He. Kenan Isik conducted research on controller development, experimental execution and data analysis. Joseph Ho mentored and coordinated the physical embodiment of the actuator; Luis Sentis mentored and coordinated the controller design, experimental execution and data analysis.

Conflicts of Interest: The authors declare no conflict of interest.

References

1. Pratt, G.A.; Williamson, M.M. Series Elastic Actuators. In Proceedings of the IEEE/RSJ International Conference on Intelligent Robots and Systems. Human Robot Interaction and Cooperative Robots, Pittsburgh, PA, USA, 5–9 August 1995; Volume 1, pp. 399–406.
2. Arumugom, S.; Muthuraman, S.; Ponselvan, V. Modeling and Application of Series Elastic Actuators for Force Control Multi Legged Robots. *J. Comput.* **2009**, *1*, 26–33.
3. Paluska, D.; Herr, H. Series Elasticity and Actuator Power Output. In Proceedings of the IEEE International Conference on Robotics and Automation, Orlando, FL, USA, 15–19 May 2006; pp. 1830–1833.
4. Lagoda, C.; Schou, A.C.; Stienen, A.H.; Hekman, E.E.; van der Kooij, H. Design of an Electric Series Elastic Actuated Joint for Robotic Gait Rehabilitation Training. In Proceedings of the 3rd IEEE RAS and EMBS International Conference on Biomedical Robotics and Biomechatronics (BioRob), Tokyo, Japan, 26–29 September 2010; pp. 21–26.
5. Diftler, M.A.; Mehling, J.; Abdallah, M.E.; Radford, N.A.; Bridgwater, L.B.; Sanders, A.M.; Askew, R.S.; Linn, D.M.; Yamokoski, J.D.; Permenter, F.; et al. Robonaut 2—The First Humanoid Robot in Space. In Proceedings of the IEEE International Conference on Robotics and Automation (ICRA), Shanghai, China, 9–13 May 2011; pp. 2178–2183.
6. Sergi, F.; Accoto, D.; Carpino, G.; Tagliamonte, N.L.; Guglielmelli, E. Design and Characterization of a Compact Rotary Series Elastic Actuator for Knee Assistance during Overground Walking. In Proceedings of the 4th IEEE RAS & EMBS International Conference on Biomedical Robotics and Biomechatronics (BioRob), Rome, Italy, 24–27 June 2012; pp. 1931–1936.
7. Lu, J.; Haninger, K.; Chen, W.; Tomizuka, M. Design and Torque-Mode Control of a Cable-Driven Rotary Series Elastic Actuator for Subject-Robot Interaction. In Proceedings of the IEEE International Conference on Advanced Intelligent Mechatronics (AIM), Banff, AB, Canada, 12–15 July 2015; pp. 158–164.
8. Veneman, J.F.; Ekkelenkamp, R.; Kruidhof, R.; van der Helm, F.C.; van der Kooij, H. A Series Elastic- and Bowden-Cable-Based Actuation System for Use as Torque Actuator in Exoskeleton-Type Robots. *Int. J. Rob. Res.* **2006**, *25*, 261–281.
9. Torres-Jara, E.; Banks, J. *A Simple and Scalable Force Actuator*; Technical Report, DTIC Document; Defense Technical Information Center: Fort Belvoir, VA, USA, 2005.
10. Sensinger, J.W.; Burkart, L.E.; Pratt, G.A.; Weir, R.F. Effect of Compliance Location in Series Elastic Actuators. *Robotica* **2013**, *31*, 1313–1318.
11. Kong, K.; Bae, J.; Tomizuka, M. A Compact Rotary Series Elastic Actuator for Human Assistive Systems. *IEEE/ASME Trans. Mechatron.* **2012**, *17*, 288–297.
12. Taylor, M.D. A Compact Series Elastic Actuator for Bipedal Robots with Human-Like Dynamic Performance. Ph.D. Thesis, Carnegie Mellon University, Pittsburgh, PA, USA, 2011.

13. Mathijssen, G.; Cherelle, P.; Lefeber, D.; Vanderborght, B. Concept of a Series-Parallel Elastic Actuator for a Powered Transtibial Prosthesis. *Actuators* **2013**, *2*, 59–73.
14. dos Santos, W.M.; Caurin, G.A.; Siqueira, A.A. Design and control of an active knee orthosis driven by a rotary Series Elastic Actuator. *Control Eng. Pract.* **2015**, doi:10.1016/j.conengprac.2015.09.008.
15. Tsagarakis, N.G.; Laffranchi, M.; Vanderborght, B.; Caldwell, D.G. A Compact Soft Actuator Unit for Small Scale Human Friendly Robots. In Proceedings of the IEEE International Conference on Robotics and Automation, Kobe, Japan, 12–17 May 2009; pp. 4356–4362.
16. Hurst, J.W.; Chestnutt, J.E.; Rizzi, A. The actuator with mechanically adjustable series compliance. *IEEE Trans. Robot.* **2010**, *26*, 597–606.
17. Grebenstein, M.; Albu-Schäffer, A.; Bahls, T.; Chalon, M.; Eiberger, O.; Friedl, W.; Gruber, R.; Haddadin, S.; Hagn, U.; Haslinger, R.; et al. The DLR Hand Arm System. In Proceedings of the IEEE International Conference on Robotics and Automation (ICRA), Shanghai, China, 9–13 May 2011; pp. 3175–3182.
18. Jafari, A.; Tsagarakis, N.G.; Caldwell, D.G. A novel intrinsically energy efficient actuator with adjustable stiffness (AwAS). *IEEE ASME Trans. Mechatron.* **2013**, *18*, 355–365.
19. Tonietti, G.; Schiavi, R.; Bicchi, A. Design and Control of a Variable Stiffness Actuator for Safe and Fast Physical Human/Robot Interaction. In Proceedings of the IEEE International Conference on Robotics and Automation, Barcelona, Spain, 18–22 April 2005; pp. 526–531.
20. Van Ham, R.; Vanderborght, B.; Van Damme, M.; Verrelst, B.; Lefeber, D. MACCEPA, the mechanically adjustable compliance and controllable equilibrium position actuator: Design and implementation in a biped robot. *Rob. Auton. Syst.* **2007**, *55*, 761–768.
21. Wolf, S.; Hirzinger, G. A New Variable Stiffness Design: Matching Requirements of the Next Robot Generation. In Proceedings of the IEEE International Conference on Robotics and Automation, Pasadena, CA, USA, 19–23 May 2008; pp. 1741–1746.
22. Thorson, I.; Caldwell, D. A Nonlinear Series Elastic Actuator for Highly Dynamic Motions. In Proceedings of the IEEE/RSJ International Conference on Intelligent Robots and Systems (IROS), San Francisco, CA, USA, 25–30 September 2011; pp. 390–394.
23. Groothuis, S.; Carloni, R.; Stramigioli, S. A Novel Variable Stiffness Mechanism Capable of an Infinite Stiffness Range and Unlimited Decoupled Output Motion. *Actuators* **2014**, *3*, 107–123.
24. Laffranchi, M.; Chen, L.; Kashiri, N.; Lee, J.; Tsagarakis, N.G.; Caldwell, D.G. Development and Control of a Series Elastic Actuator Equipped with a Semi Active Friction Damper for Human Friendly Robots. *Rob. Auton. Syst.* **2014**, *62*, 1827–1836.
25. Mooney, L.; Herr, H. Continuously-Variable Series-Elastic Actuator. In Proceedings of the IEEE International Conference on Rehabilitation Robotics (ICORR), Seattle, WA, USA, 24–26 June 2013; pp. 1–6.
26. Paine, N.; Oh, S.; Sentis, L. Design and Control Considerations for High-Performance Series Elastic Actuators. *IEEE/ASME Trans. Mechatron.* **2014**, *19*, 1080–1091.
27. Edsinger-Gonzales, A.; Weber, J. Domo: A Force Sensing Humanoid Robot for Manipulation Research. In Proceedings of the 4th IEEE/RAS International Conference on Humanoid Robots, Santa Monica, CA, USA, 10–12 November 2004; Volume 1, pp. 273–291.
28. Gregorio, P.; Ahmadi, M.; Buehler, M. Design, Control, and Energetics of An Electrically Actuated Legged Robot. *IEEE Trans. Syst. Man Cybern. B Cybern.* **1997**, *27*, 626–634.
29. Pratt, J.; Pratt, G. Intuitive Control of a Planar Bipedal Walking Robot. In Proceedings of the IEEE International Conference on Robotics and Automation, Leuven, Belgium, 16–20 May 1998; Volume 3, pp. 2014–2021.
30. Pratt, J.E.; Krupp, B.T. *Series Elastic Actuators for Legged Robots. Defense and Security. International Society for Optics and Photonics*; SPIE: Bellingham, WA, USA, 2004; pp. 135–144.
31. Hutter, M.; Remy, C.D.; Siegwart, R. *Design of an Articulated Robotic Leg with Nonlinear Series Elastic Actuation*; World Scientific: Singapore, 2009.
32. Kong, K.; Bae, J.; Tomizuka, M. Control of Rotary Series Elastic Actuator for Ideal Force-Mode Actuation in Human–Robot Interaction Applications. *IEEE ASME Trans. Mechatron.* **2009**, *14*, 105–118.
33. Ragonesi, D.; Agrawal, S.; Sample, W.; Rahman, T. Series Elastic Actuator Control of a Powered Exoskeleton. In Proceedings of the Annual International Conference of the IEEE Engineering in Medicine and Biology Society, Boston, MA, USA, 30 August–3 September 2011; pp. 3515–3518.

34. Quigley, M.; Asbeck, A.; Ng, A. A Low-Cost Compliant 7-DOF Robotic Manipulator. In Proceedings of the IEEE International Conference on Robotics and Automation (ICRA), Boston, MA, USA, 30 August–3 September 2011; pp. 6051–6058.
35. Campbell, E.; Kong, Z.C.; Hered, W.; Lynch, A.J.; Malley, M.K.; McLurkin, J. Design of a Low-Cost Series Elastic Actuator for Multi-Robot Manipulation. In Proceedings of the IEEE International Conference on Robotics and Automation (ICRA), Shanghai, China, 9–13 May 2011; pp. 5395–5400.
36. Catalano, M.G.; Grioli, G.; Garabini, M.; Bonomo, F.; Mancini, M.; Tsagarakis, N.; Bicchi, A. Vsa-Cubebot: A Modular Variable Stiffness Platform for Multiple Degrees of Freedom Robots. In Proceedings of the IEEE International Conference on Robotics and Automation (ICRA), Shanghai, China, 9–13 May 2011; pp. 5090–5095.
37. Baxter. Redefining Robotics and Manufacturing. Available online: http://www.rethinkrobotics.com/baxter/ (accessed on 5 September 2016).
38. Nash-Hoff, M. Viewpoint: Why is China Cheaper? Available online: http://www.industryweek.com/environment/viewpoint-why-china-cheaper (accessed on 28 April 2016).
39. Low Pass Filter For Derivative Control. Available online: https://chess.eecs.berkeley.edu/tbd/wiki/C-code/LowPassFilterForDerivativeControl (accessed on 28 April 2016).
40. Haddadin, S.; Albu-Schaffer, A.; De Luca, A.; Hirzinger, G. Collision Detection and Reaction: A Contribution to Safe Physical Human-Robot Interaction. In Proceedings of the IEEE/RSJ International Conference on Intelligent Robots and Systems, Nice, France, 22–26 September 2008; pp. 3356–3363.
41. De Luca, A.; Flacco, F. Integrated Control for pHRI: Collision Avoidance, Detection, Reaction and Collaboration. In Proceedings of the 4th IEEE RAS & EMBS International Conference on Biomedical Robotics and Biomechatronics (BioRob), Rome, Italy, 24–27 June 2012; pp. 288–295.